THERMAL CONDUCTIVITY OF NAFION MOLECULAR CHAIN BASED ON FIRST-PRINCIPLE CALCULATION

Yi-Nan Nie, Lei Chen, & Wen-Quan Tao*

Key Laboratory of Thermal-Fluid Science and Engineering, Ministry of Education, Xi'an Jiaotong University, Xianning West Road No. 28, Xi'an Shannxi, 710049, China

*Address all correspondence to: Lei Chen, Key Laboratory of Thermal-Fluid Science and Engineering, Ministry of Education, Xi'an Jiaotong University, Xianning West Road No. 28, Xi'an Shannxi, 710049, China, E-mail: chenlei@xjtu.edu.cn

Original Manuscript Submitted: 11/28/2019; Final Draft Received: 3/13/2020

The thermal conductance in Nafion molecular chain is investigated by VASP, Phonopy, and ShengBTE based on the first-principle calculation. By using the mechanical structural analysis and chemical bond analysis of crystal orbital overlap population, the strength of carbon–carbon bond, carbon–oxygen bond, and carbon–sulfur bond is discussed. Combined with the pDOS (phonon density of state) analysis, we have determined that the backbone linked by carbon–carbon bonds is always the main route of phonon transport in the Nafion molecular chain, and the branches with sulfonate ions also play a non-negligible phonon transfer role in the local molecular chains. The results of thermal conductivity calculation prove the above analysis that the thermal conductivity of the Nafion molecular chain is much higher than that of the bulk/membrane, but still at a lower level [< 7 W/(m·K)]. The relationship between the structure and thermal conductivity is further discussed by comparing the Nafion structure and exemplary two-dimensional material structure (silicene and $^{12}C/^{13}C$ graphene superlattice).

KEY WORDS: *first principle, density functional theory, phonon transfer, Nafion molecular chain, thermal conductivity*

1. INTRODUCTION

The proton exchange membrane fuel cell (PEMFC) has been recognized as a reliable alternative to the fossil fuels machine for its high energy density and low emission. Though a great deal of work has been done in the studies of PEMFC by researchers, there are still many mechanistic problems that need to be discussed before PEMFC can be widely applied to industries (Hassanzadeh and Mansouri, 2005; Deevanhxay et al., 2011; Burheim et al., 2015; García-Salaberri et al., 2015; Fiori et al., 2015; Fazeli et al., 2016; Epting and Litster, 2016; Nandjou et al., 2016; Zhang et al., 2017; Gao et al., 2017). One of the most concerning problems is the thermal management of the fuel cell. The thermal conductivity of the proton exchange membrane is a key parameter in the fuel cell heat transfer process, however, there is lack of research about Nafion thermal conductivity to the best of the authors' knowledge.

The most commonly used material of the proton exchange membrane is Nafion invented by Dupont Corporation, which is a typical porous polymer. Due to the complex microstructure of Nafion, the internal heat conduction mechanism becomes very complicated.

Scholars use the transient plane source method extensively to conduct experimental measurements of dry Nafion thermal conductivity at 25^{o}C by a hot disk thermal constants analyzer (ISO22007-2, 2008; Zhang et al., 2010, 2013a,b; Wang et al., 2010). Some self-developed experimental systems are also used to measure the thermal conductivity of Nafion. Khandelwal and Mench (2006) performed the *in situ* direct measurement of Nafion through-plane thermal conductivity over a range of temperatures from 17 to 65^{o}C by a steady-state measurement method. Burheim et al. (2010) performed the *ex situ* measurements of through-plane thermal conductivity of Nafion as a function of water content.

There is a common problem with above experimental measurement methods: the measurement accuracy of the thermal conductivity of the wetted Nafion cannot be guaranteed. The experimental process of measuring thermal

conductivity takes a period of steady state, while the water content of Nafion may vary during measurement. To further solve this problem, Chen et al. (2014) studied the thermal conductivity of Nafion 117 at 25°C by the hot disk method, and established a molecular dynamics calculation model of the proton exchange membrane according to the chemical structure by Materials Studio (MS) software platform. In Chen et al. (2017), the effect of water content and temperature on the thermal conductivity is also discussed to reveal the relationship between the thermal conductivity, water content, and temperature.

The above experimental studies of Nafion membranes should be considered as macroscopic studies. Though the numerical simulations by the molecular dynamics method are generally considered as microscopic research, the modeling and calculation still focus on the problems at the macroscale such as the effect of water content and temperature on the thermal conductivity of Nafion. With the development of computational science, the focus of thermal conductivity research has gradually shifted to its relationship with the microstructure of materials, especially at the molecular and atomic scales. Based on the first-principles and calculation software packages, the thermal conductivity can also be investigated and calculated at an atomistic scale (Yan et al., 2013). In recent years, one of the hot topics in materials science is two-dimensional and one-dimensional materials. First-principles-based calculations have performed well in the research on the thermal conductivity of low-dimensional materials (Ma et al., 2012, 2017; Lee et al., 2014).

In this paper, we try to work out the relationship between the heat conductance performance and the microstructure of Nafion. Since the Nafion bulk is agglomerated by long molecular chains, its microscopic thermal conduction mechanism includes the mechanism of the thermal conduction in Nafion molecular chain and the mechanism of energy transfer between the molecular chains. Both these two parts will be mentioned in this paper.

2. DETAILS OF NUMERICAL SIMULATION

2.1 Molecular Model

The molecular formula and the long molecular chain model are shown in Fig. 1. The protrusion on the carbon–fluorine backbone (marked out by red circle in Fig. 1) is carbon branches with the sulfate ions (SO_3^-), which are connected to the backbone through two carbon–oxygen C–O bonds and reduce the balance of molecular chains. Two different models of Nafion molecular chain part are given in Fig. 2 as two basic calculation models of this paper. The key principle is that the chosen molecular chain must contain the branch with the sulfonate as it determines many of Nafion material properties, such as hydrophilicity, proton transfer ability, and so on. In this kind of branch, there will be two C–O bonds, which is also the basis for selecting and judging the branches.

2.2 Computational Details

Thermal conductivity is defined as the amount of heat transferred by a unit temperature gradient over a unit heat conduction surface in a unit time. The macrocalculation method of thermal conductivity is the Fourier law of heat

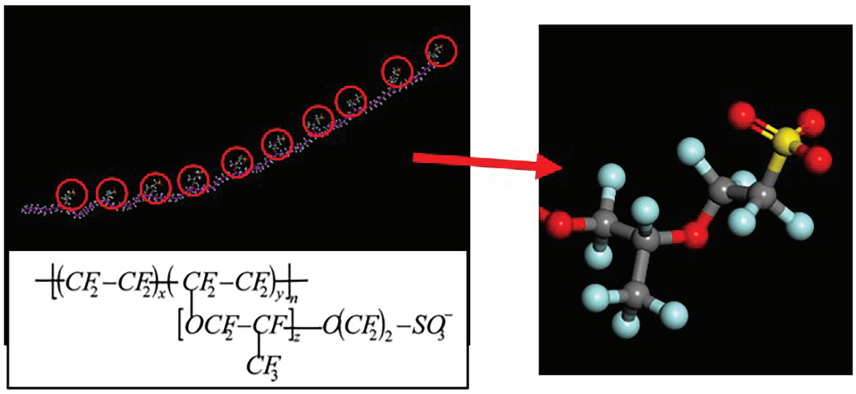

FIG. 1: The structure of Nafion molecular long chain: (a) minimal Nafion molecule ($C_9F_{17}S_1O_5$), (b) Nafion molecule with carbon chain ($C_{21}F_{41}S_1O_5$)

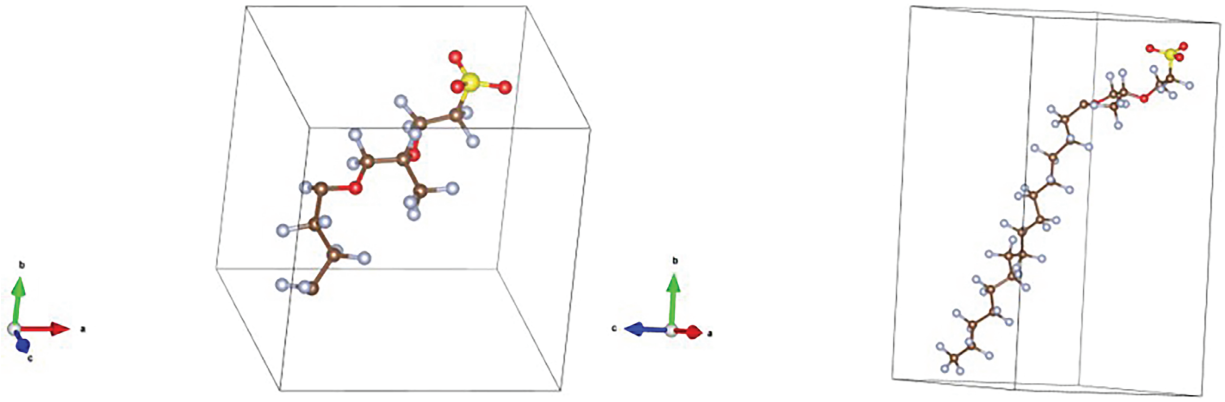

FIG. 2: The structure of Nafion molecular chain part

conduction. The thermal conductivity microcalculation method in this paper is to solve the phonon Boltzmann transport equation (BTE) using calculation software packages. The calculation software packages used in this paper are VASP, Phonopy (Togo et al., 2008), and ShengBTE (Li et al., 2014), which are used for density functional calculation, phonon calculation, and thermal conductivity calculation, respectively. The brief calculation flowchart is shown in Fig. 3, which is provided and proven by Li et al. (2014). This method has been recognized and used by many scholars, especially proving ShengBTE as an effective solver to phonon Boltzmann transport equation (Carrete et al., 2014; Qin et al., 2015; Xie et al., 2016; Shafique and Shin, 2017).

In the structural calculation, we use the VASP package to optimize the structure of two Nafion molecular chains with limit of truncation energy on 600 eV and residual as 1.0×10^{-6} eV. Since the lattice vectors of three dimensions are larger than 15 Å, the structural relaxation is done for the unit cell with a $1 \times 1 \times 1$ Monkhorst–Pack grid of k sampling. Two important input files of ShengBTE, the second-order (harmonic) and third-order (anharmonic) interatomic force constants (IFCs), are calculated by Phonopy and the thirdorder.py script packaged with ShengBTE. The $2 \times 1 \times 1$ supercell with $20 \times 1 \times 1$ k sampling for Brillouin zone integration is used for IFCs calculation. After the harmonic and anharmonic interatomic force constants are calculated and symmetrized, the phonon Boltzmann transport equation (Ziman, 1960) is then solved to obtain the thermal conductivity of Nafion molecular chain.

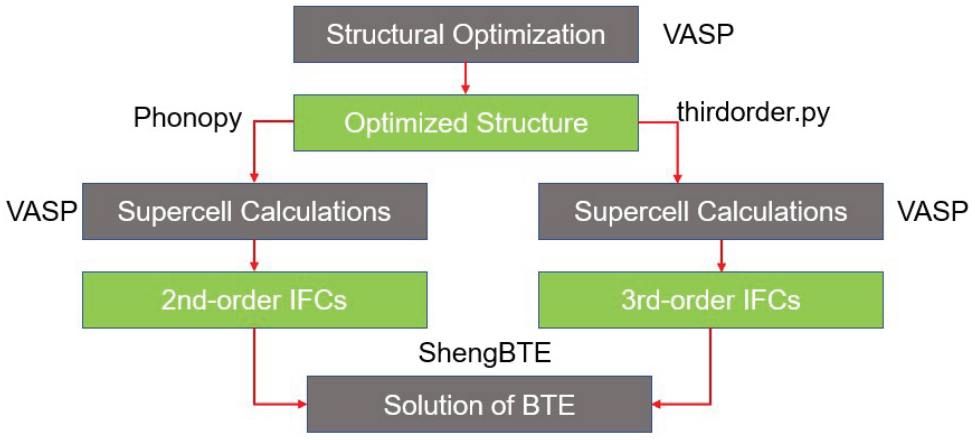

FIG. 3: Calculation flow diagram

2.2.1 Kohn–Sham Equation

The calculations performed by VASP are based on the density functional theory (DFT), and the key equation used is the Kohn–Sham equation (Bylaska et al., 2009). The Kohn–Sham equation refers to the Schrödinger equation that the virtual system associated with the real system satisfies in the density functional theory. The particles (usually electrons) in the virtual system move in an effective potential field without interaction, and the particle density is the same as the real system at each point in space. The effective potential in the Kohn–Sham equation is usually $v_s(r)$ or $v_{\text{eff}}(r)$ to express, called the Kohn–Sham potential. The particles in the virtual system are fermions that do not interact with each other, so the exact solution of the Kohn–Sham equation is a single Slater determinant, and the orbit in the determinant is called the Kohn–Sham orbit. Each Kohn–Sham track can be expressed as a linear combination of atomic orbitals; it can also be expanded according to a basis function. The form of the Kohn–Sham equation is as follows:

$$\left(-\frac{\hbar^2}{2m}\nabla^2 + v_{\text{eff}}\left(r\right)\right)\phi_i\left(r\right) = \varepsilon_i\phi_i\left(r\right), \tag{1}$$

where ε_i is the orbital energy of the Kohn–Sham track ϕ_i. The electron density of the Kohn–Sham system containing N particles is given by

$$\rho\left(r\right) = \sum_{i}^{N}\left|\phi_i\left(r\right)\right|^2 \quad . \tag{2}$$

2.2.2 Selection of Potential

The three potentials used in VASP calculations are the mode of conservation, the ultrasoft potential, and the projector augmented wave (PAW) potential. According to different methods, these potentials can be divided into ultrasoft pesudopotential (USPP) and PAW. Both methods can reduce the number of plane waves of the transition metal or each atom of the first row element to a certain extent. According to the exchange correlation function, it is divided into local density approximation (LDA) and generalized-gradient approximation (GGA). GGA is divided into Perdew–Wang 91 (PW91) and Perdew–Burke–Ernzerhof (PBE). The electronic structure at *Rc* is calculated as a uniform electron gas of the same density in the local density functional LDA, while the gradient of density is considered the generalized gradient functional GGA to get higher accuracy. Therefore, in this study, the potential of S (sulfur), C (carbon), F (fluorine), and O (oxygen) is the PAW–GGA–PBE potential in the paw_pbe folder provided by VASP.

2.2.3 Phonon Boltzmann Transport Equation

A nonzero heat current J is caused by the temperature gradient (Li et al., 2014):

$$J = \sum_{p}\int f_\lambda \hbar\omega_\lambda v_\lambda \frac{dq}{\left(2\pi\right)^3}, \tag{3}$$

where λ includes both a phonon branch index p and a wave vector q, ω_λ, and v_λ are the angular frequency and group velocity of phonon mode λ, respectively, and f_λ is the phonon distribution function.

The phonons in thermal equilibrium (there is no temperature gradient and other thermodynamic forces) are distributed according to the Bose–Einstein statistic $f_0(\omega\lambda)$. When there is a temperature gradient, the deviation of phonon actual distribution function f_λ from $f_0(\omega\lambda)$ in equilibrium can be obtained by BTE. The BTE considers two factors affecting phonon distribution: diffusion and scattering, and explains the fact that the rate of change of phonon distribution inevitably disappears in a steady state (Peierls, 1929; Li et al., 2014):

$$\frac{df_\lambda}{dt} = \left.\frac{\partial f_\lambda}{\partial t}\right|_{\text{diffusion}} + \left.\frac{\partial f_\lambda}{\partial t}\right|_{\text{scattering}} = 0, \tag{4}$$

where

$$\left.\frac{\partial f_\lambda}{\partial t}\right|_{\text{diffusion}} = -\nabla T \cdot v_\lambda \frac{\partial f_\lambda}{\partial T}, \tag{5}$$

and $\left.\partial f_\lambda \middle/ \partial t\right|_{\text{scattering}}$ depends on the actual scattering situation, which can be analyzed by the perturbation theory.

Most of the time, the norm of ∇T is small enough that f_λ can be first-order extended in ∇T and expressed as $f_\lambda = f_0(\omega\lambda) + g_\lambda$. And the linear relationship between g_λ and ∇T can be expressed as $g_\lambda = -F_\lambda \cdot \nabla T \cdot df_0/dT$. When the scattering sources are the two- and three-phonon processes, the linearized BTE can then be written as (Omini and Sparavigna, 1995, 1996; Lindsay and Broido, 2008; Ward and Broido, 2010; Ward et al., 2009)

$$F_\lambda = \tau_\lambda^0 \left(v_\lambda + \Delta_\lambda\right). \tag{6}$$

2.2.4 Nanowires Correction

The structure of a nanowire can be viewed as extending only in one dimension, and its phonon dispersion should be expressed as a function of the wavenumber along that direction. When the nanowire is thick enough, it will contain a large number of unit cells in the radial direction, that is, there are a large number of phonon branches. The bulk phonon dispersions can be used instead, though the translational symmetry perpendicular to the nanowire axis is still destroyed by physical boundaries. Then the BTE needs to supplement a spatial correlation term and correct Eq. (6) to (Li et al., 2012, 2014):

$$F_{r,\lambda} = \tau_\lambda^0 \left\{\Delta_{r,\lambda} + v_\lambda \left[1 - \frac{1}{|v_\lambda|^2}\left(v_\lambda \cdot \nabla\right)\left(v_\lambda \cdot F_{r,\lambda}\right)\right]\right\}. \tag{7}$$

3. RESULTS AND DISCUSSION

3.1 Structure and Chemical Bonding Analysis

After structural relaxation, the carbon–carbon (C–C) bond average length is 1.5 Å, the carbon–sulfur (C–S) bond length is 1.46 Å, and the carbon–oxygen (C–O) bond length is 1.42 Å. These structure parameters are in good agreement with the experimental results (Doyle and Rajendran, 2003), which suggests that the structures after relaxation are reliable. To move a step further, a series of crystal orbital overlap population (COOP) analyses are carried out by LOBSTER (as shown in Fig. 4), an open-source program developed by the Dronskowski group at RWTH Aachen University (Dronskowski and Blöchl, 1993; Deringer et al., 2012; Maintz et al., 2014, 2016). COOP is calculated by multiplying overlapping populations by corresponding states density, can also be expressed as overlapping population-weighted density of states. The integral value of COOP below the Fermi level can be understood as the number of bonding electrons shared between two atoms, which can reflect the strength of the bond. In the analysis, the range of the energy is selected as –18 eV to 12 eV, and we fitted the figures with the range of COOP from –0.2 to 0.4.

As mentioned above, it is the area below the Fermi level that we mainly care about in the COOP figure. In this area, the peaks with the positive COOP values represent the bonding which indicates that the chemical bond is stronger, while the peaks with the negative COOP values represent the antibonding. As we can tell, the C–C bonding, the S–O bonding, and the C–O bonding all got several antibonding which we do not expect. The COOP values of antibonding are all in the range of –0.1–0 and very close. In the comparison, the C–C bonding is the strongest bonding of the three bondings since it has 2 significant positive peaks with the COOP value about 0.3, while the C–O bonding seems to be the weakest of the three bondings as it got the lowest COOP value.

Back to the structure of Nafion molecular chain, the C–C bonding is the main bonding of the Nafion backbone, the C–O bonding and the C–S bonding play the role of connecting the sulfate ions branches to the C–F backbone. From the perspective of energy/phonon transmission, weak chemical bonds do not provide positive conditions for efficient phonon transfer, which indicates the Nafion molecular chain may not have high thermal conductivity.

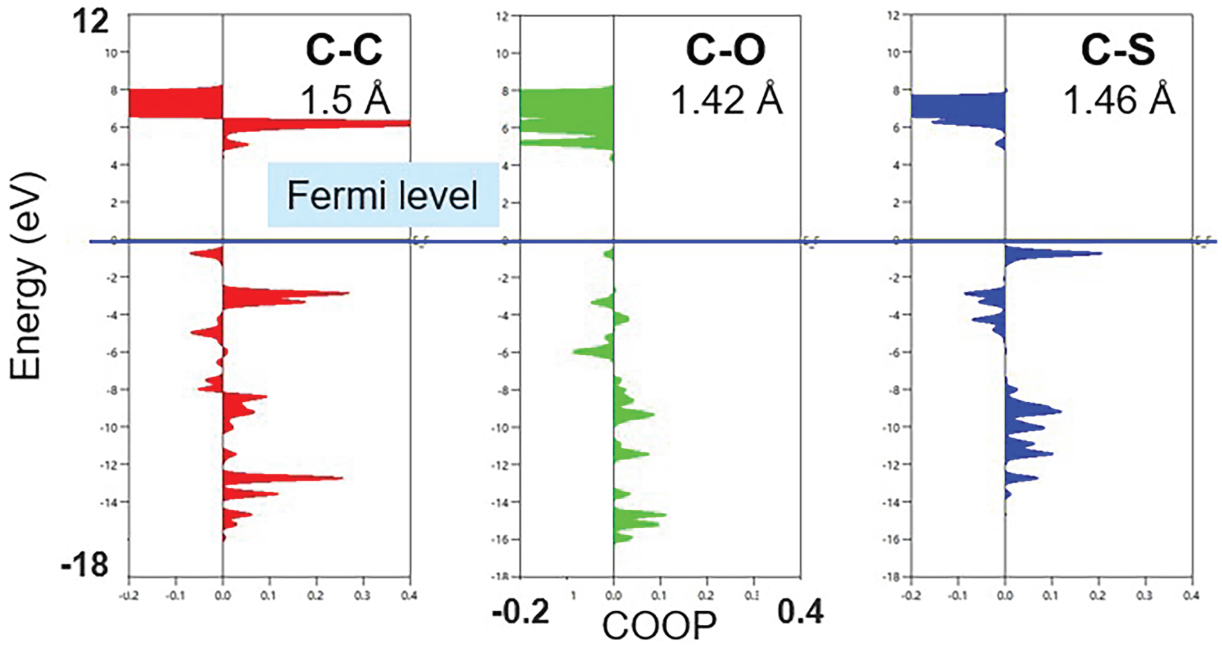

FIG. 4: COOP analysis of C–C bond, C–O bond, and C–S bond

3.2 Thermal Conductance Analysis

First, the distribution of phonon density at different frequencies is performed by Phonopy. As shown in Fig. 5, the density of state has two obvious peaks in the lower frequency (about 1 THz) and higher frequency (about 33 THz). Due to the stability of the C–C bond and the fluorocarbon backbone connected by C–C bonds, the DOS peak at low frequencies is formed by the C–C bond as the main influencing factor. The backbone and the sulfonate group are connected by two C–O bonds, and the branch is used as the extension of the main chain, and the vibration frequency is high. Therefore, the DOS peak near 33 THz is caused by this part of the branch. Regardless of the molecular mass or the strength of the chemical bond, as the molecular chain grows, the influence of the branch on the phonon transfer will naturally decrease. However, in the two molecular chains, we calculated, the effect of the branches including the SO_3^- to the thermal conductance still cannot be ignored.

In the final output of ShengBTE, the thermal conductivity per unit of mean free path (in the small-grain limit) of the two molecular chains remains almost the same as 0.065 W/(m·K·nm). The definition of the thermal conductivity per unit of mean free path is the local thermal conductivity in the mean phonon free path range, which is directly related to the microstructure of the material. The phonon free path of each material is different, which means that the phonon transmission performance of different materials is also different. The same result of the thermal conductivity per unit of mean free path of the two molecules in this paper also proves the structural consistency. In Table 1, the thermal conductivities of Nafion bulk/membrane (according to Chen's research) and molecular chain are shown. As we can tell, the thermal conductivities of molecular chains have a significant rise compared with the bulk/membrane, but still remain at a low level with the order of magnitude of 10, confirming the above analysis and conjecture.

3.3 Analysis of the Relationship between Structure and Thermal Conductivity

As we can tell, both the Nafion bulk and the Nafion molecular chain have rather low thermal conductivity. Compared to some two-dimensional/one-dimensional materials with high thermal conductivity, we can find some patterns of the relationship between structure and thermal conductivity.

Most of the two-dimensional/one-dimensional materials with excellent heat transfer performance have the mechanical structural stability, and the mechanical structural stability is based on the typical unit as lattice structure.

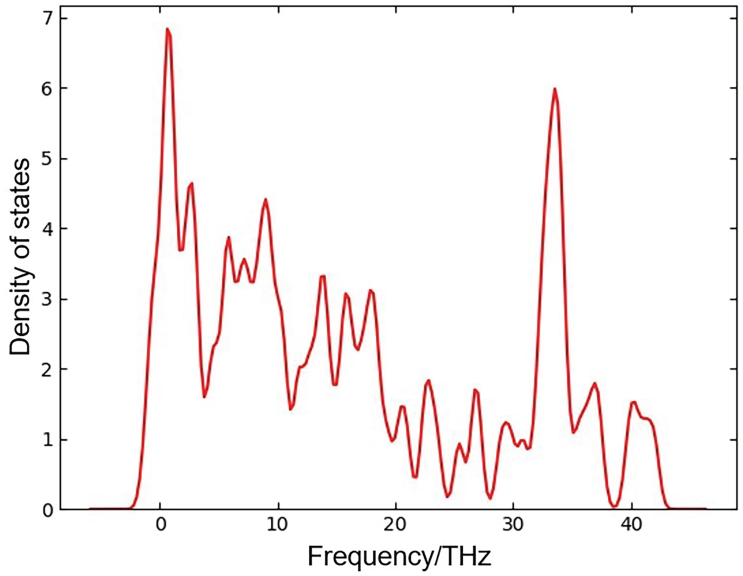

FIG. 5: PDOS (phonon density of state) figure of the minimal Nafion molecule

TABLE 1: Comparison of thermal conductivity between Nafion membrane and molecular chain at 300 K

Bulk/Membrane		**Molecular Chain**	
MD	Experiment	$C_9F_{17}S_1O_5$	$C_{21}F_{41}S_1O_5$
0.12 W/(m·K)	0.14 W/(m·K)	6.73 W/(m·K)	4.17 W/(m·K)

In the examples given in this paper, as shown in Fig. 6, the two materials—silicone (Liu et al., 2017) and $^{12}C/^{13}C$ graphene superlattice (Mu et al., 2015)—mainly consist of a hexagonal silicon ring and a hexagonal carbon ring. On this basis, the material layer is formed by such a unit to a two-dimensional periodic expanding. This kind of structure ensures the overall mechanical stability, which means the bonds in the materials have high strength. In

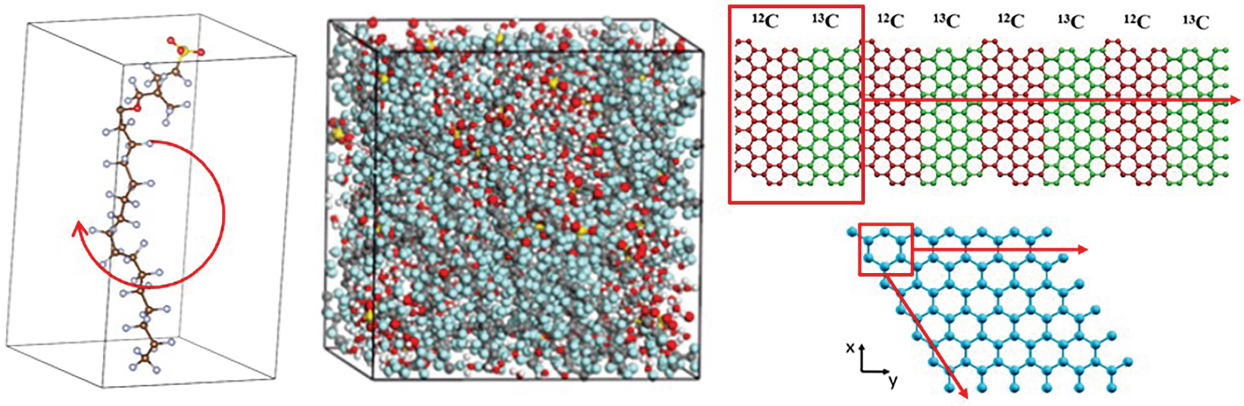

FIG. 6: Comparison of Nafion structure with exempliary two-dimensional material structure

contrast to the analysis given in Sections 3.2 and 3.3, stable chemical bonds not only ensure the mechanical properties of the material, but also provide thermal stability to the material.

Moving on to the Nafion microstructure, as an amorphous polymer compound with linear structural molecular chain, the form of its formation is fundamentally different from the above two-dimensional materials. Nafion bulk/membrane is agglomerated by molecular chains, and this causes a great number of interfaces between the molecular chains. This kind of interfaces can be approximately considered as crystal defect, which means that Nafion can be considered a high defect crystal, phonon scattering at the defect will become a key factor in the thermal resistance of the material. Focusing on a single Nafion molecular chain, it will also show the characteristic of amorphous polymer, the backbone connected by carbon bonds has no regular fold line arrangement, and the molecular chain may twist and bend while forming Nafion bulk/membrane. The irregular composition of the internal molecular chains results in poor thermal stability and poor heat transfer performance, while exhibiting certain anisotropic properties. Lin et al. (2017) also found that the thermal conductivity of amorphous polyethylene can be raised to the theoretical limit by using the CG–MD method to simulate hot stretching process. This study shows that the thermal conductivity of the polymer is positively correlated with its molecular chain order and polymer crystallinity, which is consistent with the conclusion of the above analysis. When the molecular arrangement inside the polymer tends to be ordered, and its structure tends to be stable, which is conducive to the transfer of energy.

The intuitive general conclusions drawn above can be theoretically explained by the following three points. These three points summarize the general characteristics of materials with intrinsically low thermal conductivity. Combining the above analysis of the structural characteristics of Nafion, the relationship between the Nafion microstructure the low thermal conductivity can be further stated:

1) Strong anharmonicity. The strength of anharmonicity is mainly related to the symmetry of the chemical bond and the equilibrium position of the atom. During the vibration of an atom, the greater the deviation of its symmetry center, the stronger the asymmetry. As mentioned, Nafion molecular chain structure lacks symmetry and is easy to twist and deform so that the Nafion molecular chain has strong anharmonicity.
2) Weak chemical bonds. Materials with weak chemical bonds have lower phonon velocities, atoms have more active space near their equilibrium positions, and electron cloud distribution is more diffuse. In the phonon spectrum, weak chemical bonds often correspond to some low-frequency phonon modes, which are more likely to couple with the acoustic branch, thereby further reducing the contribution of the acoustic branch to the thermal conductance. COOP analysis in this article proves that the weak chemical bond strength in Nafion molecular chain will also reduce its thermal conductivity.
3) Complex unit cell structure. On the one hand, the contribution of the acoustic branch to the total heat transfer capacity can be reduced due to complex unit cell structure, and on the other hand, the group velocity of the acoustic branch phonons can be reduced. As the Nafion bulk/membrane is agglomerated by molecular chains, its structure does not have any periodicity or symmetry. The complexity of its cell structure is also one of the reasons for low thermal conductivity.

4. CONCLUSIONS

In conclusion, we have performed first-principle calculation to study the phonon and thermal transport properties of the Nafion molecular chain:

(1) Structure and chemical bonding analysis are carried out by crystal orbital overlap population (COOP), the order of the strength of the main chemical bonds that make up the Nafion molecular chain is: carbon–carbon bond > carbon–sulfur bond > carbon–oxygen bond.
(2) Phonon density of state shows that the backbone linked by carbon–carbon bonds is always the main route of phonon transport in the Nafion molecular chain, and the branch of the sulfonate chain also plays a non-negligible phonon transfer roll in the local molecular chains.
(3) The calculated thermal conductivities of $C_9F_{17}S_1O_5$ and $C_{21}F_{41}S_1O_5$ are 6.73 W/(m·K) and 4.17 W/(m·K), which have a significant rise than the thermal conductivity of the Nafion bulk/membrane [0.12–0.14 W/(m·K)]. Despite this, the molecular thermal conductivity is still at a low level, but this calculation result proves the above-mentioned conjecture analysis of the influence of sulfonate branch on thermal conductivity.
(4) Comparing the structure of Nafion with two high thermal conductivity two-dimensional materials (silicene and $^{12}C/^{13}C$ graphene superlattice), it is found that the high anharmonicity, weak chemical bonds, and complex cell structure caused by the irregular microstructure of Nafion are the root causes of the low thermal conductivity of Nafion bulk/membrane.

ACKNOWLEDGMENT

This work has been supported by the National Natural Science Foundation of China (Grant No. 51876161).

REFERENCES

Burheim, O., Vie, P.J.S., and Pharoah, J.G., *Ex Situ* Measurements of Through-Plane Thermal Conductivities in a Polymer Electrolyte Fuel Cell, *J. Power Sources*, vol. **195**, no. 1, pp. 249–256, 2010.

Burheim, O.S., Crymble, G.A., Bock, R., Hussain, N., Pasupathi, S., and du Plessis, A., Thermal Conductivity in the Three Layered Regions of Micro Porous Layer Coated Porous Transport Layers for the PEM Fuel Cell, *Int. J. Hydrogen Energy*, vol. **40**, no. 46, pp. 16775–16785, 2015.

Bylaska, E.J., Holst, M., and Weare, J.H., Adaptive Finite Element Method for Solving the Exact Kohn–Sham Equation of Density Functional Theory, *J. Chem. Theor. Comput.*, vol. **5**, no. 4, pp. 937–948, 2009.

Carrete, J., Mingo, N., and Curtarolo, S., Low Thermal Conductivity and Triaxial Phononic Anisotropy of SnSe, *Appl. Phys. Lett.*, vol. **105**, no. 10, 101907, 2014.

Chen, L., He, Y.L., and Tao, W.Q., The Temperature Effect on the Diffusion Processes of Water and Proton in the Proton Exchange Membrane Using Molecular Dynamics Simulation, *Numer. Heat Transf., Part A*, vol. **65**, pp. 216–228, 2014.

Chen, L., Nie, Y.N., Wang, S.Y., and Tao, W.Q., The Experimental Study on Thermal Conductivity of Composite Proton Exchange Membrane, *ICCM2017*, Xi'an, China, 2017.

Deevanhxay, P., Sasabe, T., Tsushima, S., and Hirai, S., Investigation of Water Accumulation and Discharge Behaviors with Variation of Current Density in PEMFC by High-Resolution Soft X-Ray Radiography, *Int. J. Hydrogen Energy*, vol. **36**, no. 17, pp. 10901–10907, 2011.

Deringer, V.L., Tchougreeff, A.L., and Dronskowski, R., Crystal Orbital Hamilton Population (COHP) Analysis as Projected from Plane-Wave Basis Sets, *J. Phys. Chem. A*, vol. **115**, pp. 5461–5466, 2012.

Doyle, M. and Rajendran, G., *Handbook of Fuel Cells Fundamentals, Technology and Applications*, Chichester: John Wiley & Sons, pp. 340–355, 2003.

Dronskowski, R. and Blöchl, P.E., Crystal Orbital Hamilton Populations (COHP). Energy-Resolved Visualization of Chemical Bonding in Solids Based on Density-Functional Calculations, *J. Phys. Chem.*, vol. **97**, pp. 8617–8624, 1993.

Epting, W.K. and Litster, S., Microscale Measurements of Oxygen Concentration across the Thickness of Diffusion Media in Operating Polymer Electrolyte Fuel Cells, *J. Power Sources*, vol. **306**, pp. 674–684, 2016.

Fazeli, M., Hinebaugh, J., Fishman, Z., Tötzke, C., Lehnert, W, and Manke, I., Pore Network Modeling to Explore the Effects of Compression on Multiphase Transport in Polymer Electrolyte Membrane Fuel Cell Gas Diffusion Layers, *J. Power Sources*, vol. **335**, pp. 162–171, 2016.

Fiori, C., Dell'Era, A., Zuccari, F., Santiangeli, A., D'Orazio, A., and Orecchini, F., Critical Review of Fuel Cell's Membranes and Identification of Alternative Types for Automotive Applications, *Int. J. Hydrogen Energy*, vol. **40**, no. 35, pp. 11949–11959, 2015.

Gao, Y., Montana, A., and Chen, F., Evaluation of Porosity and Thickness on Effective Diffusivity in Gas Diffusion Layer, *J. Power Sources*, vol. **342**, pp. 252–265, 2017.

García-Salaberri, P.A., Gostick, J.T., Hwang, G., Weber, A.Z., and Vera, M., Effective Diffusivity in Partially-Saturated Carbon-Fiber Gas Diffusion Layers: Effect of Local Saturation and Application to Macroscopic Continuum Models, *J. Power Sources*, vol. **296**, pp. 440–453, 2015.

Hassanzadeh, H. and Mansouri, S., Efficiency of Ideal Fuel Cell and Carnot Cycle from a Fundamental Perspective, *Proc Inst. Mech. Eng., Part A, J. Power Energy*, vol. **219**, no. 4, pp. 245–254, 2005.

ISO22007-2, Plastics—Determination of Thermal Conductivity and Thermal Diffusivity—Part 2: Transient Plane Heat Source (Hot Disc) Method, 2008.

Khandelwal, M. and Mench, M.M., Direct Measurement of Through-Plane Thermal Conductivity and Contact Resistance in Fuel Cell Materials, *J. Power Sources*, vol. **161**, no. 2, pp. 1106–1115, 2006.

Lee, S., Esfarjani, K., Luo, T.F., Zhou, J.W., Tian, Z.T., and Chen, G., Resonant Bonding Leads to Low Lattice Thermal Conductivity, *Nat. Commun.*, vol. **5**, 3525, 2014.

Li, W., Carrete Jesús, A., and Katcho, N., ShengBTE: A Solver of the Boltzmann Transport Equation for Phonons, *Comput. Phys. Commun*., vol. **185**, no. 6, pp. 1747–1758, 2014.

Li, W., Mingo, N., Lindsay, L., Broido, D.A., Stewart, D.A., and Katcho, N.A., Thermal Conductivity of Diamond Nanowires from First Principles, *Phys. Rev. B*, vol. **85**, 195436, 2012.

Lin, S.C., Shih, C.J., Sresht, V., Rajan, A.G., Strano, M.S., and Blankschtein, D., Understanding the Colloidal Dispersion Stability of 1D and 2D Materials: Perspectives from Molecular Simulations and Theoretical Modeling, *Adv. Colloid Interface Sci.*, vol. **244**, pp. 36–53, 2017.

Lindsay, L. and Broido, D.A., Three-Phonon Phase Space and Lattice Thermal Conductivity in Semiconductors, *J. Phys.: Condens. Matter*, vol. **20**, no. 16, 165209, 2008.

Liu, Z.Y., Wu, X.F., and Luo, T.F., The Impact of Hydrogenation on the Thermal Transport of Silicone, *2D Materials*, vol. **4**, no. 2, 025002, 2017.

Ma, F., Zheng, H.B., Sun, Y.J., Yang, D., Xu, K.W., and Chu, P.K., Strain Effect on Lattice Vibration, Heat Capacity, and Thermal Conductivity of Graphene, *Appl. Phys. Lett.*, vol. **101**, no. 11, 2012.

Ma, L., Mei, R.G., Liu, M.G., Zhao, X.X., Wu, Q.X., and Sun, H.Y., Monte Carlo Simulation of Single-Crystalline PbSe Nanowire Thermal Conductivity Using First-Principle Phonon Properties, *Semiconductor Sci. Technol.*, vol. **32**, no. 9, 2017. DOI: 10.1088/1361-6641/aa7c15

Maintz, S., Deringer, V.L., Tchougreeff, A.L., and Dronskowski, R., Analytic Projection from Plane-Wave and PAW Wavefunctions and Application to Chemical-Bonding Analysis in Solids, *J. Comput. Chem.*, vol. **34**, pp. 2557–2567, 2014.

Maintz, S., Deringer, V.L., Tchougreeff, A.L., and Dronskowski, R., LOBSTER: A Tool to Extract Chemical Bonding from Plane-Wave Based DFT, *J. Comput. Chem.*, vol. **37**, pp. 1030–1035, 2016.

Mu, X., Zhang, T., Go, D.B., and Luo, T.F., Coherent and Incoherent Phonon Thermal Transport in Isotopically Modified Graphene Superlattices, *Carbon*, vol. **83**, pp. 208–216, 2015.

Nandjou, F., Poirot-Crouvezier, J.P., Chandesris, M., Rosini, S., Hussey, D.S., and Jacobson, D.L., A Pseudo-3D Model to Investigate Heat and Water Transport in Large Area PEM Fuel Cells E. Part 2: Application on an Automotive Driving Cycle, *Int. J. Hydrogen Energy*, vol. **41**, no. 34, pp. 15573–15584, 2016.

Omini, M. and Sparavigna, A., An Iterative Approach to the Phonon Boltzmann Equation in the Theory of Thermal Conductivity, *Physica B*, vol. **212**, pp. 101–112, 1995.

Omini, M. and Sparavigna, A., Beyond the Isotropic-Model Approximation in the Theory of Thermal Conductivity, *Phys. Rev. B*, vol. **53**, no. 14, pp. 9064–9073, 1996.

Peierls, R.E., Zur Kinetischen Theorie der Wärmeleitung in Kristallen, *Ann. Phys. (Leipzig)*, vol. **3**, pp. 1055–1101, 1929.

Qin, G.Z., Yan, Q.B., Qin, Z.Z., Yue, S.Y., Hu, M., and Su, G., Anisotropic Intrinsic Lattice Thermal Conductivity of Phosphorene from First Principles, *Phys. Chem. Chem. Phys.*, vol. **17**, no. 7, pp. 4854–4858, 2015.

Shafique, A. and Shin, Y.H., Thermoelectric and Phonon Transport Properties of Two-Dimensional IV–VI Compounds, *Sci. Rep.*, vol. **7**, 506, 2017.

Togo, A., Oba, F., and Tanaka, I., First-Principles Calculations of the Ferroelastic Transition between Rutile-Type and $CaCl_2$-Type SiO_2 at High Pressures, *Phys. Rev. B*, vol. **78**, no. 13, 134106, 2008.

Wang, W.W., Min, Z., Li, L.Z., and Liu, Q.J., Measurement Methods and Technology of Thin-Film Thermal Conductivity, *J. Funct. Mater.*, vol. **41**, no. 5, pp. 870–873, 2010.

Ward, A. and Broido, D.A., Intrinsic Phonon Relaxation Times from First-Principles Studies of the Thermal Conductivities of Si and Ge, *Phys. Rev. B*, vol. **81**, 085205, 2010.

Ward, A., Broido, D.A., Stewart, D.A., and Deinzer, G., *Ab Initio* Theory of the Lattice Thermal Conductivity in Diamond, *Phys. Rev. B*, vol. **80**, 125203, 2009.

Xie, H., Ouyang, T., Germaneau, E., Qin, G.Z., Hu, M., and Bao, H., Large Tunability of Lattice Thermal Conductivity of Monolayer Silicene via Mechanical Strain, *Phys. Rev. B*, vol. **93**, 075404, 2016.

Yan, R.S., Simpson, J.R., Bertolazzi, S., Brivio, J., Watson, M., Wu, X.F., Kis, A., Luo, T.F., Walker, A.R.H., and Xing, H.G., Thermal Conductivity of Monolayer Molybdenum Disulfide Obtained from Temperature-Dependent Raman Spectroscopy, *ACS Nano*, vol. **8**, no. 1, pp. 986–993, 2014.

Zhang, H., Jin, Y., and Gu, W., A Numerical Study on the Influence of Insulating Layer of the Hot Disk Sensor on the Thermal Conductivity Measuring Accuracy, *Prog. Comput. Fluid Dyn., Int. J.*, vol. **13**, nos. 3–4, pp. 191–201, 2013.

Zhang, H., Li, M.J., Fang, W.Z., He, Y.L., and Tao, W.Q., A Numerical Study on the Theoretical Accuracy of Film Thermal Conductivity Using Transient Plane Source Method, *Appl. Therm. Eng.*, vol. **72**, no. 1, pp. 62–69, 2013.

Zhang, J.S., Yang, J.Y., Zhu, W., Xiao, C.J., Zhang, H., and Peng, J.Y., Research Advances in the Measurement for the Thermal Conductivity of Thin Solid Films, *Mater. Rev.*, vol. **24**, no. 7, pp. 103–107, 2010.

Zhang, X.F., Yang, D.J., Luo, M.H., and Dong, Z.M., Load Profile Based Empirical Model for the Lifetime Prediction of an Automotive PEM Fuel Cell, *Int. J. Hydrogen Energy*, vol. **42**, no. 16, pp. 11868–11878, 2017.

Ziman, J.M., *Electrons and Phonons: The Theory of Transport Phenomena in Solids*, Gloucestershire: Clarendon Press, 1960.